ACS NANO Cite This: ACS Nano XXXX, XXX, XXX-XXX www.acsnano.org

ARTICLE

Self-Assembled Colloidal Gel Using Cell Membrane-Coated Nanosponges as Building Blocks

Yue Zhang,[†,‡] Weiwei Gao,[†,‡] Yijie Chen,[†,‡] Tamara Escajadillo,[§,∥] Jessica Ungerleider,[⊥,#] Ronnie H. Fang,[†,‡] Karen Christman,[⊥,#] Victor Nizet,[§,∥] and Liangfang Zhang*[,†,‡]

[†]Department of Nanoengineering, [‡]Moores Cancer Center, [§]Department of Pediatrics, [∥]Skaggs School of Pharmacy and Pharmaceutical Sciences, [⊥]Department of Bioengineering, and [#]Sanford Consortium for Regenerative Medicine, University of California San Diego, La Jolla, California 92093, United States

Supporting Information

ABSTRACT: **Colloidal gels consisting of oppositely charged nanoparticles are increasingly utilized for drug delivery and tissue engineering. Meanwhile, cell membrane-coated nanoparticles are becoming a compelling biomimetic system for innovative therapeutics. Here, we demonstrate the successful use of cell membrane-coated nanoparticles as building blocks to formulate a colloidal gel that gelates entirely based on material self-assembly without chemical cross-linking. Specifically, we prepare red blood cell membrane-coated nanosponges and mix them with an appropriate amount of cationic nanoparticles, resulting in a spontaneously formed gel-like complex. Rheological test shows that the nanosponge colloidal gel has pronounced shear-thinning property, which makes it an injectable formulation. The gel formulation not only preserves the nanosponges' toxin neutralization capability but also greatly prolongs their retention time after subcutaneous injection into mouse tissue. When tested in a mouse model of subcutaneous group A *Streptococcus* infection, the nanosponge colloidal gel shows significant antibacterial efficacy by markedly reducing skin lesion development. Overall, the nanosponge colloidal gel system is promising as an injectable formulation for therapeutic applications such as antivirulence treatment for local bacterial infections.**

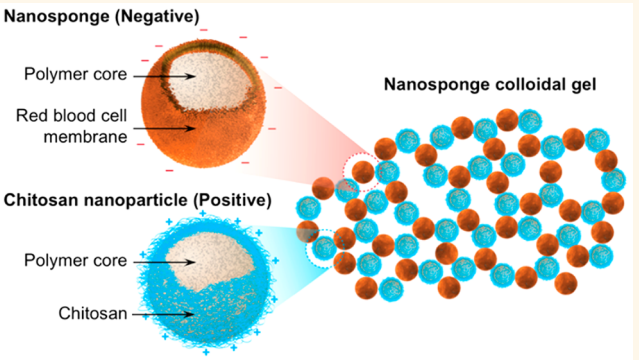

KEYWORDS: *colloidal gel, nanosponge, self-assembly, detoxification, bacterial infection*

Colloidal gels comprise a continuous network of particles assembled through strong, yet transient and reversible, electrostatic charge interactions.[1,2] With compelling shear-thinning and self-healing characteristics, they are becoming an important class of biomaterials with broad applications.[1,3] Recently, the use of therapeutic nanoparticles as building blocks to formulate colloidal gels is gaining attention in drug delivery and tissue engineering applications.[4,5] Polymeric nanoparticles have distinct engineering flexibility for tailored physicochemical properties such as size, charge, and surface chemistry; therefore, they offer a simple route to assemble highly tunable gel-like materials while avoiding complex molecular design and synthesis.[6,7] The resulting nanoparticle colloidal gels confer two levels of structural hierarchy, namely the polymer chain network within each nanoparticle and the cross-linked nanoparticle assembly, which together provide advanced control over drug release kinetics.[8] Compared to bulk hydrogel systems, nanoparticle colloidal gels can effectively alleviate mass transport barriers within the gel network without compromising bulk mechanical strength. As a result, these advanced biomaterials exhibit a fast response to local chemical cues for triggered drug release.[9] In addition, colloidal gels made with high concentrations of nanoparticles exhibit pseudoplastic behavior desirable for fabricating moldable and shape-specific materials.[10] Notably, when constructed of biocompatible and biodegradable materials, these colloidal gels have high potential for tissue regeneration.[11] Together, these multiple advantages make nanoparticle-based colloidal gels a promising class of biomaterials.

Multifunctional nanoparticle design for therapeutic applications has made considerable progress in recent years.[12,13] One emerging approach is the use of natural cell membranes to coat

Received: October 1, 2017
Accepted: November 8, 2017
Published: November 8, 2017

DOI: 10.1021/acsnano.7b06968
ACS Nano XXXX, XXX, XXX−XXX

synthetic nanoparticles for biofunctionalization.[14−16] In this approach, intact plasma membranes are collected from natural cells and then wrapped onto nanoparticle surfaces. The resulting cell membrane-coated nanoparticles inherit and display natural surface antigens and associated functions while preserving the highly tunable physicochemical properties of synthetic nanomaterials.[17] This "top-down" fabrication makes it possible to replicate complex biological interfaces present in nature to confer sophisticated nanoparticle functionality without exposure to foreign materials or unfavorable chemical reactions. Following this approach, nanoparticles have been coated with membranes derived from various cell types including red blood cells (RBCs), platelets, cancer cells, leukocytes, and bacteria.[14,16,18−20] These biomimetic nanoparticles have inspired a wide range of innovations in areas such as detoxification, drug delivery, and vaccination.[21−23] Interestingly, regardless of their diverse biological identity and functionality, cell membrane-coated nanoparticles in general carry a net negative surface charge inherited from their source membranes. Therefore, they may spontaneously engage in electrostatic charge interactions with cationic materials without the need for further modification.[17,24] This feature motivated us to hypothesize that cell membrane-coated nanoparticles could be used as building blocks to construct colloidal gels. If so, this conceptual framework could allow creation of colloidal gels that combine biomimetic functionalities with cohesive network properties.

To test our hypothesis, we first fabricated RBC membrane-coated nanoparticles (also referred to as "nanosponges", here denoted "RBC-NPs") by coating RBC membranes onto polymeric cores made from poly(lactic-*co*-glycolic acid) (PLGA) (Figure 1A). At the same time, we prepared companion chitosan-functionalized PLGA nanoparticles that possessed a similar size but opposite surface charge (denoted "Chi-NPs"). Upon mixing, these two oppositely charged nanoparticles self-assembled, forming a cohesive 3D network or "nanosponge colloidal gel" (denoted "NC-gel"). When applied with an external shear force, the NC-gel demonstrated shear-thinning behavior; however, upon removal of the external force, its strong cohesive properties recovered. Such reversible network stability is attributable to the transient disruption of interparticle interactions, indicating a successful colloidal gel formation.

Notably, prior work with RBC-NPs harnessed their capability to absorb and neutralize structurally diverse bacterial pore-forming toxins for therapeutic administration as antivirulence agents.[15,23,25] When embedded into covalently cross-linked hydrogels for injection, the RBC-NPs effectively neutralized secreted bacterial toxins to impede the development of local infection.[26] In the present study, we fabricate a NC-gel pairing RBC-NPs and Chi-NPs and achieve significantly prolonged retention of RBC-NPs in both biological buffers and mouse subcutaneous tissues without the need for chemical conjugation. *In vitro*, the NC-gel retained the full capacity to inhibit toxin-induced hemolysis seen with RBC-NPs alone, indicating that the gel formulation preserves the critical biological functionality of the RBC-NPs. In a mouse model of subcutaneous infection with the toxin-producing human bacterial pathogen group A *Streptococcus* (GAS), the NC-gel showed significant therapeutic efficacy, as evidenced by markedly diminished bacterial skin lesion development. Overall, we have successfully used cell membrane-coated nanoparticles as building blocks to formulate NC-gel entirely based on material self-assembly without chemical cross-linking. The colloidal gel system demonstrated significant potential as an injectable formulation for medical applications including antivirulence therapy against localized bacterial infection.

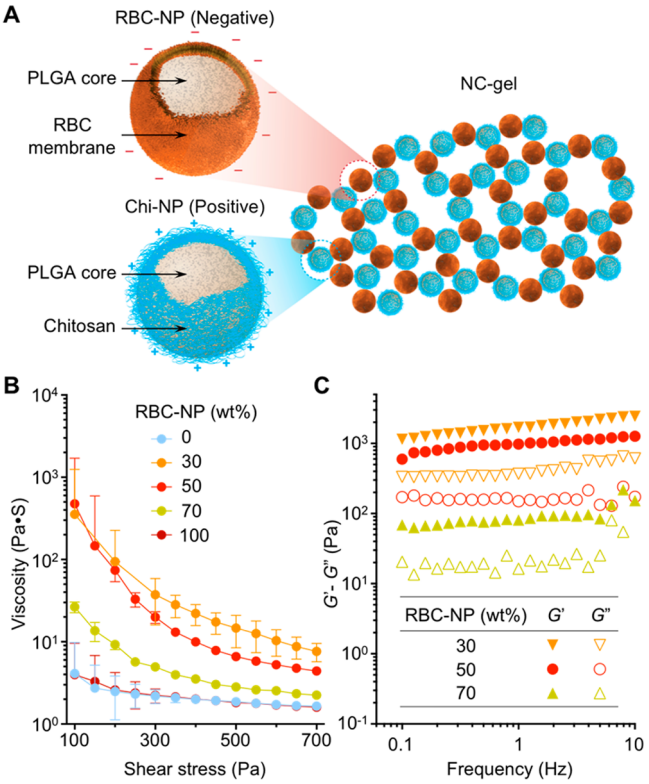

Figure 1. Preparation of nanosponge colloidal gel (denoted "NC-gel"). (A) Schematic illustration of NC-gel formulation by mixing red blood cell membrane-coated nanoparticles (RBC-NPs), which possess a negative surface charge, with chitosan-modified nanoparticles (Chi-NPs) as positively charged nanoparticle counterparts. (B) RBC-NPs and Chi-NPs mixed at different mass ratios (0, 30, 50, 70, and 100 wt % of RBC-NPs) were measured for viscosity with varying shear stress (100−700 Pa). (C) RBC-NPs and Chi-NPs mixed at different mass ratios (30, 50, and 70 wt % of RBC-NPs) were measured for the storage modulus G' and loss modulus G'' against frequency (0.1−10 Hz). All rheological measurements were performed at 25 °C.

RESULTS AND DISCUSSION

In the study, RBC-NPs (nanosponges) were prepared by coating membranes derived from human RBCs onto PLGA polymeric cores through a sonication process.[27] The resulting RBC-NPs exhibited a hydrodynamic diameter of 150.9 ± 0.8 nm and a surface ζ-potential of −22.3 ± 1.7 mV. Meanwhile, to prepare Chi-NPs, an acetone solution containing PLGA was added dropwise into an aqueous solution of chitosan.[28] The subsequent acetone evaporation led to the formation of Chi-NPs with a diameter of 194.3 ± 1.8 nm and a surface charge of 34.2 ± 0.4 mV. Following the preparations, we directly mixed the two oppositely charged nanoparticles at a fixed mass concentration (20 wt %, PLGA polymer content) but varied the mass ratios of the nanoparticle components. Each formulation was examined for its rheological characteristics. In steady flow measurements, nanoparticle suspensions containing RBC-NP or Chi-NP alone showed low viscosity with minimum shear-thinning behavior (Figure 1B and Table S1 in Supporting

DOI: 10.1021/acsnano.7b06968
ACS Nano XXXX, XXX, XXX−XXX

Information). In contrast, a significant increase in viscosity was observed when two nanoparticles were mixed, revealing the occurrence of strong attractive electrostatic charge interactions between the two colloids. Notably, viscosity values measured from the sample with an equal mass ratio of the colloids (50 wt % of RBC-NP and 50 wt % of Chi-NPs) were slightly lower than that calculated for the sample with a RBC-NP concentration of 30 wt %. This likely reflects the smaller absolute value of ζ-potential of negatively charged RBC-NPs compared to that of Chi-NPs, which means that a more equivalent overall charge balance is achieved when the Chi-NPs are provided in excess.[10]

Viscous mixtures were further examined with dynamic rheological measurements of the storage modulus (G') and the loss modulus (G'') as a function of frequency (Figure 1C). In all three samples, G' exceeded the corresponding G'' over the entire frequency range tested, and both moduli showed weak dependence on frequency, implying the dominance of a gel-like viscoelastic behavior.[29] Results from steady flow and dynamic measurements were consistent: the mixture with higher viscosity also possessed higher values for the corresponding moduli. When adjusted to 1× PBS, values of G' and G'' decreased as the ionic strength increased, suggesting an active role of electrostatic interaction in NC-gel formulation (Figure S1 in Supporting Information). For the subsequent studies, we specifically selected a NC-gel that contained equal masses of RBC-NPs and Chi-NPs (50 wt % of each) because this formulation has high viscosity, pronounced shear-thinning behavior, and a substantial fraction of nanosponges as the active component for detoxification.

We next characterized the NC-gel to verify its cohesive network properties. Colloidal gels consisting of oppositely charged nanoparticles are known to exhibit pseudoplastic characteristics, which facilitate the formation of materials with defined shapes under static conditions.[8,10] Indeed, the suspensions of single component RBC-NPs or Chi-NPs were fluid-like and unable to form a defined 3D structure when placed onto a substrate. In contrast, the NC-gel retained a freestanding 3D structure, implying a critical function of its internal charge interactions for maintaining the overall cohesive properties of the colloidal assembly (Figure 2A and Figure S2 in Supporting Information). In addition, consecutive acceleration sweeping with a shear force revealed nearly identical viscosity profiles, indicating an excellent recovery of the NC-gel architecture upon the removal of the external shear force (Figure 2B and Table S2 in Supporting Information). The NC-gel was also examined for its microscopic morphology. In the study, RBC-NPs and Chi-NPs were labeled with red (DiD) and green (DiO) fluorescent dyes, respectively, and the resulted NC-gel sample was examined by laser scanning confocal microscopy (LSCM, Figure 2C). In ambient conditions, the fluorescent imaging showed the two distinct nanoparticle components to be clearly distinguishable. In addition, the green and red signals were evenly distributed, indicating the homogeneous mixing of both nanoparticle components. The imaging also revealed long-range ring- and branch-like structures. When zoomed in, a representative fluorescence image shows that the nanoparticle agglomerates were connected to form a porous structure (Figure 2D). To further characterize these microscopic structures, the NC-gel sample was dried and examined under a scanning electron microscope (SEM). The ultrastructure exhibited a porous morphology with nanoparticles linked into loosely organized circular structures

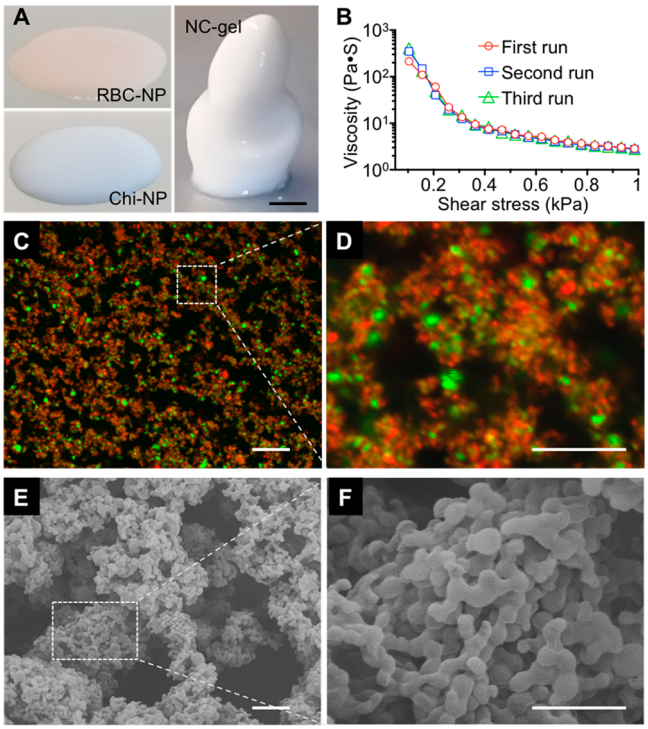

Figure 2. Characterization of the NC-gel. (A) Images of RBC-NPs, Chi-NPs, and NC-gel samples when they were placed onto a flat substrate. Scale bar = 5 mm. (B) Viscosity measurements were performed on the same NC-gel sample at 25 °C for three consecutive runs without interval between each run. (C) Representative fluorescence image of the NC-gel, in which RBC-NPs were labeled with DiD dye (red) and Chi-NPs with DiO dye (green). Scale bar = 1 μm. (D) Zoomed-in image of the marked area in (C). Scale bar = 10 μm. (E) Representative SEM image of the NC-gel. Scale bar = 1 μm. (F) Zoomed-in SEM image of the marked area in (E). Scale bar = 0.5 μm.

(Figure 2E). In a representative zoomed-in image, domains of more tightly packed nanoparticle agglomerates and open pores were seen (Figure 2F). The observed NC-gel morphology, which features mixed agglomerates and pores, also matches previous studies on nanoparticle colloidal gel systems, implying the cohesive nature of NC-gel as a result of the interplay between nanoparticle attraction (agglomerates) and repulsion (pores).[9,10] Overall, the structural retention under static conditions, excellent shear-thinning behavior, and microscopic characterizations collectively suggest the successful formation of colloidal gels using RBC-NPs as building blocks.

For local administration and treatment, prolonged retention of RBC-NPs by using the gel formulation is desirable. We hypothesized that the electrostatic attractions among oppositely charged nanoparticle building blocks of NC-gel would prolong RBC-NP retention under physiological conditions and began by examining RBC-NP diffusion out of the NC-gel network *in vitro*. In this study, the NC-gel was formulated with fluorescently labeled RBC-NPs and loaded into a dialysis chamber equipped with pores of 1 μm in diameter. The release of RBC-NPs was monitored by measuring the fluorescence intensity outside of the dialysis chamber. For comparison, RBC-NPs alone were used as a control. Within 24 h, the NC-gel released 1.3 ± 1.5% of the total RBC-NPs, a negligible amount compared to 80.8 ± 11.1% measured from the pure RBC-NP suspension control (Figure 3A). This sharp contrast in

DOI: 10.1021/acsnano.7b06968
ACS Nano XXXX, XXX, XXX−XXX

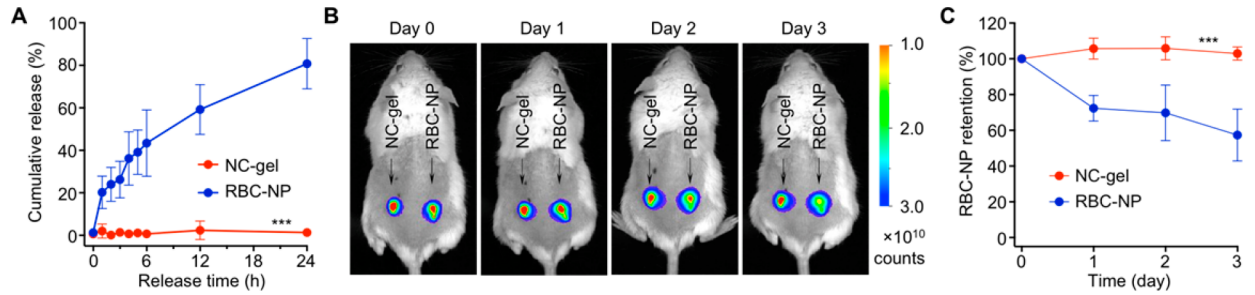

Figure 3. RBC-NP retention within the NC-gel. (A) Cumulative release of RBC-NPs measured from the NC-gel and RBC-NP suspension. RBC-NP was labeled with DiD dye, and samples were placed in dialysis chambers equipped with filters with 1 μm pore size. (B) Fluorescence images of mice injected with NC-gel and RBC-NP samples. NC-gel was formulated with DiD-labeled RBC-NPs. The samples were injected subcutaneously under the loose skin over the left flank of the mice. RBC-NPs alone without mixing with Chi-NPs were injected as a control over the right flank of the same mice. Fluorescence images were taken on days 0, 1, 2, and 3 after the injection. (C) Quantification of the fluorescence intensity as observed in (B). All images are representative of three mice from each group, and error bars represent the standard deviation (n = 3); ***P < 0.001.

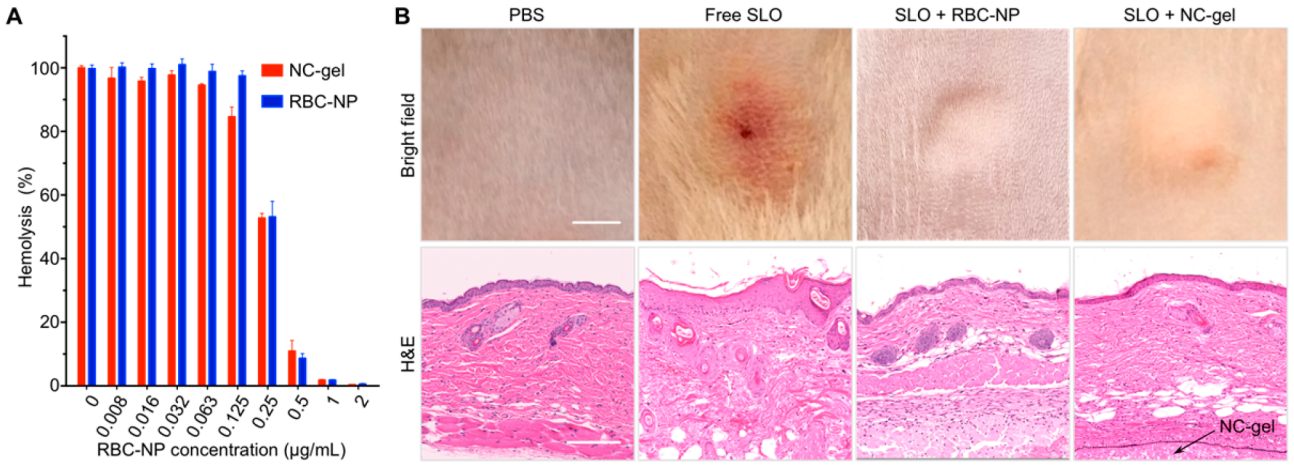

Figure 4. Evaluation of toxin neutralization capability of the NC-gel *in vitro* and *in vivo*. (A) *In vitro* neutralization of Streptolysin-O (SLO) by the NC-gel and free RBC-NPs to inhibit toxin-induced hemolysis. In all samples, SLO concentration was maintained at 1 μg/mL, and the concentration of RBC-NP component was varied. (B) *In vivo* neutralization of SLO. Free SLO, SLO + RBC-NP, or SLO + NC-gel was injected subcutaneously into CD-1 mice. Mice injected with PBS only served as a control group. Mice injected with free SLO developed skin lesions after 3 days, but no lesions were observed for mice in other treatment groups (scale bar = 20 mm). Hematoxylin and eosin (H&E) stained histological sections revealed inflammatory infiltrate, apoptosis, necrosis, and edema in the epidermis for the SLO-treated mice. In contrast, mice in other groups showed no abnormality in the epidermis (scale bars = 0.2 mm).

nanoparticle release indicates that the NC-gel can effectively immobilize and retain RBC-NPs within its network. We then investigated retention of the RBC-NPs within the gel under *in vivo* conditions. NC-gel samples containing fluorescently labeled RBC-NPs were injected subcutaneously into the left flank of mice. As a control, samples containing the same quantity of free RBC-NPs were injected to the right flank of the same mice. Following the injection, whole-body imaging of the mice revealed the confinement of fluorescence at the injection sites (Figure 3B). In the study, a faster decay of fluorescence intensity was observed at sites injected with free RBC-NPs compared to sites injected with the NC-gels, indicating a more rapid loss of nanoparticles through diffusion to surrounding tissues. Quantification of the fluorescence intensity showed that 30.0 ± 15.5% of the free RBC-NPs diffused away from the injection site by day 2 and 42.6 ± 14.5% by day 3. In contrast, the NC-gel formulation showed negligible loss of RBC-NPs during the full 3 day testing period (Figure 3C), demonstrating the prolonged retention of RBC-NPs achieved with NC-gel formulation. Compared to previous studies that used acrylate-based hydrogels for nanoparticle encapsulation and retention, the current approach achieves enhanced nanoparticle retention, relying entirely on physical self-assembly without any chemical processing.[26,29]

RBC nanosponges have shown capabilities to absorb and neutralize various pore-forming toxins. In this study, we selected this property as a functional assay to test whether the NC-gel formulation retained key biological functionality of the entrapped nanosponges. To do so, we selected the well-characterized GAS toxin, Streptolysin-O (SLO), as a model pore-forming toxin and tested the ability of the NC-gel to inhibit SLO-induced hemolytic activity compared to free RBC-NPs. An SLO concentration of 1 μg/mL was utilized because at this concentration the toxin causes complete cell lysis. Recombinant SLO was mixed with serial dilutions of NC-gel or RBC-NPs prior to mixing with freshly purified human RBCs. As shown in Figure 4A, in both groups, as the concentration of RBC-NP increased, the degree of RBC hemolysis was correspondingly reduced. Specifically, 50% inhibition of hemolysis was achieved with an RBC-NP concentration of approximately 0.25 mg/mL and a nearly 100% inhibition observed with a RBC-NP concentration of 1 mg/mL. At all

DOI: 10.1021/acsnano.7b06968
ACS Nano XXXX, XXX, XXX−XXX

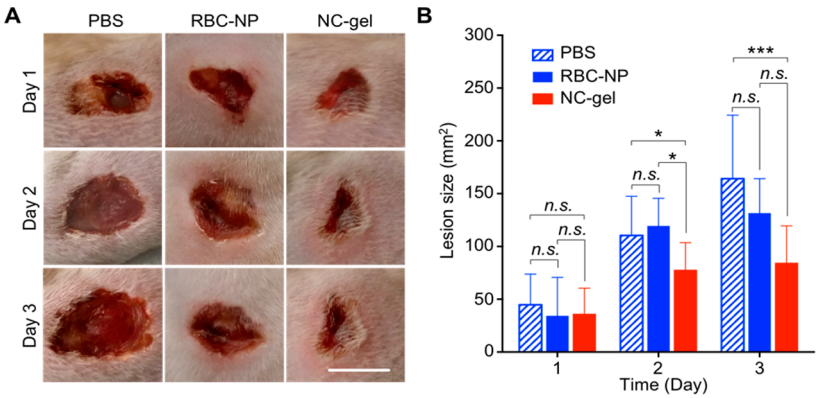

Figure 5. Evaluation of the NC-gel for protecting mice from group A *Streptococcus* (GAS) infection *in vivo*. To establish GAS infection, 2×10^9 CFU of GAS bacteria were injected subcutaneously under the loose skin on the back of the mice (n = 6 per group). Immediately after injection of the bacteria, PBS, RBC-NP alone, or NC-gel was injected to the infection site. (A) Skin lesions were monitored and photographed on days 1, 2, and 3 after the injection (scale bar = 1 cm). (B) Lesion sizes were measured and compared among the groups. Bars represent median values (*P < 0.05, ***P < 0.001, ns: not significant). Statistical analysis was performed with two-way ANOVA followed by Tukey posthoc test in GraphPad Prism.

tested concentrations, the NC-gel sample showed inhibition efficiency without significant difference compared to that of free RBC-NPs, suggesting that the NC-gel formulation retains the full neutralization capability of its component RBC-NPs upon gelation.

Neutralization of SLO by NC-gel was further tested *in vivo* (Figure 4B). In the study, SLO toxin was mixed with NC-gel and free RBC-NPs and then injected into the loose flanks of the mice. Mice injected with SLO only and PBS served as two control groups. At 72 h after injection, mice challenged with SLO alone developed clear skin lesions characterized by localized edema and inflammation. In contrast, mice injected with the NC-gel and free RBC-NP preparations had healthy appearing skin at the injection site similar to a PBS control group. Skin biopsy sections were further analyzed with histological staining. Mouse skin treated with SLO alone showed edema within the stratum spinosum, alteration of vascular structure in the dermal layes, obvious erythrocyte extravasation, and keratinocyte necrosis. In contrast, skin treated with NC-gel, RBC-NPs, or PBS alone possessed normal epithelial structures in skin histology without discernible damages; all of these samples showed stratified squamous epithelium with intact fibrous structures and absence of erythrocyte extravasation. Similar complete toxin neutralization effects observed with the NC-gel compared to RBC-NP group *in vivo* further confirm that the neutralization function of RBC-NP is well preserved within the NC-gel formulation.

Finally, to demonstrate the therapeutic potential of the NC-gel, we tested their use as an antivirulence agent to protect mice from a live subcutaneous bacterial infection. GAS, which elaborates SLO and several other pore-forming toxins and proteases,[30,31] is a major cause of invasion to skin and soft tissue infection in humans,[32] making it a relevant model for testing the efficacy of NC-gel in local treatment. Subcutaneous GAS infection was established by injecting 2×10^9 CFU bacteria underneath the flank skin of ICR mice, randomized into three groups (n = 6 per group) for treatment with PBS, free RBC-NPs, and NC-gel. Therapeutic efficacy was evaluated by measurement of the GAS-induced skin lesion.[33,34] On day 1 after the bacterial challenge, all groups developed visible skin lesions of similar size (Figure 5A,B). However, on day 2, mice treated with the NC-gel showed significantly smaller lesions than mice injected with the PBS control. On day 3, the NC-gel group showed significant reduction of lesion size than mice treated with either PBS or free RBC-NPs. In contrast, free RBC-NPs showed no significant reduction of lesion sizes compared to the PBS control. Duration of the NC-gel potency after *in vivo* administration is likely affected by multiple factors, including gel composition, nanosponge size, core degradation rate, disease types, and route of administration. Notably, toxin neutralization by nanosponges has also been shown to protect immune cells and facilitate immune activation, which together enhance overall antibacterial immune responses for potency.[35] Nevertheless, a superior efficacy in lesion reduction observed with the NC-gel verifies its potential as an effective local treatment agent to mitigate tissue damage produced by GAS infection.

The combination of therapeutic nanoparticles with hydrogels has emerged as a novel biomaterial formulation with intriguing and versatile therapeutic application potentials.[5] However, such combinations to date have relied largely on chemical cross-linking to embed and retain nanoparticles within the gel network. From this perspective, the NC-gel reported herein provides a straightforward and gentle approach to use nanoparticles themselves as building blocks coupled with an entirely physical gelation process. The resulting NC-gel also generates a synergy between cell membrane-coated nanosponges and gel-like bulk assembly: while the nanosponges offer biomimetic toxin absorption and neutralization, the hydrogel enhances retention of the nanosponges at the site of application (*e.g.*, an infected tissue focus), which focuses localized bioactivity for enhanced efficacy. The engineering flexibility of making cell membrane-coated nanoparticles allows for a wide range of formulation preparation and optimization. For example, nanoparticles coated with membranes of mammalian cells or bacterial cells possess a negative surface charge; therefore, the approach of NC-gel formulation can be readily extended to nanoparticles coated with other types of cell membranes.[18,20] Furthermore, physicochemical properties of cell membrane-coated nanoparticles, including size, surface charge, and surface antigens, can be tailored for better biointerfacing toward specific treatment.[17,36] In addition, cell membrane-coated nanoparticles would also be expected to interact with other cationic materials such as polymers and

DOI: 10.1021/acsnano.7b06968
ACS Nano XXXX, XXX, XXX−XXX

nanofibers for self-assembly and gelation.[6,37] This powerful platform of material diversity and formulation flexibility makes the NC-gel approach broadly applicable.

CONCLUSIONS

In summary, this study introduced a framework for using cell membrane-coated nanoparticles to fabricate colloidal gels. RBC-NPs were studied as a model nanoparticle system and paired them with cationic Chi-NPs to formulate a NC-gel. This colloidal gel was optimized by varying the relative composition of the two oppositely charged nanoparticles. The resulting gel effectively retained RBC-NPs within its network without compromising their toxin neutralization capability. In a GAS subcutaneous mouse infection model, mice treated with the NC-gel showed clear reductions in skin lesion development. The reported NC-gel takes advantage of the natural surface charge of cell membranes, in general, and this formulation process is expected to be applicable to nanoparticles coated with membranes of other cell types. The formulation process is physical, facile, and chemical-free, hence allowing the NC-gel to retain functionalities without affecting the original functions of the building blocks. The resulting colloidal gel combines the biomimetic functionality from the cell membrane-coated nanoparticles with the cohesive network property from the bulk gel, together opening exciting opportunities for advanced therapeutic applications.

METHODS

Materials. Chemicals including chitosan oligosaccharide lactate (M_w = 5000), dithiothreitol (DTT), and acetone were purchased from Sigma-Aldrich. Fluorophores including 1,1′-dioctadecyl-3,3,3′,3′-tetramethylindodicarbocyanine, 4-chlorobenzenesulfonate salt (DiD, excitation/emission = 644/665 nm), and 3,3′-dioctadecyloxacarbocyanine perchlorate (DiO, excitation/emission = 484/501 nm) were purchased from ThermoFisher Scientific. Poly(lactic-*co*-glycolic) acid (50:50, 0.67 dL/g) was purchased from LACTEL Absorbable Polymers. Packed human red blood cells were purchased from ZenBio, Inc., from which cell membrane was derived according to a previously published protocol.[14]

Preparation of RBC Membrane-Coated Nanosponge Colloidal Gel. RBC-NPs were synthesized by coating bare PLGA cores with RBC membrane.[27] Briefly, to prepare bare PLGA cores, 10 mL of PLGA (20 mg/mL in acetone) was added to 20 mL of Tris-HCl buffer (10 mM, pH 8). The solution was stirred and allowed to evaporate for 2 h. For membrane coating, purified RBC membrane was first mixed with PLGA core at a protein-to-polymer weight ratio of 1:4, followed by bath sonication for 10 min. To prepare Chi-NPs, 50 mL of PLGA (4 mg/mL in acetone) was added to 100 mL chitosan solution (1 mg/mL in water) under continuous stirring, followed by evaporation for 10 h.[28] For fluorescence labeling, DiD or DiO was mixed with PLGA polymer (dye-to-polymer weight ratio = 1:40000) in acetone followed by nanoparticle preparation. RBC-NPs or Chi-NPs were collected with centrifugation (19000*g* for 20 min). The pellets were washed with DI water three times to remove excess membrane or chitosan and redispersed in deionized water to a concentration of 20% w/v. The colloidal gel was prepared by mixing the two nanoparticle suspensions at desired ratios followed by a brief bath sonication of 3 min. The resulting NC-gel was stored at 4 °C for further usage.

Characterization of NC-gel. To study the shape stability, 500 μL of NC-gel (50 wt % RBC-NP), RBC-NP (20 w/v%), or Chi-NP (20 w/v%) was extruded to a clean steel plate at ambient condition using a 1 mL syringe and photographed. The rheological analysis was carried out at 25 ± 0.1 °C on a strain-controlled AR-G2 rheometer with a 20 mm diameter parallel-plate geometry (TA Instruments Inc., New Castle, DE). The 500 μm gap was filled with the 200 μL gel samples. A solvent trap was placed around the geometry to prevent liquid evaporation during the measurements. Oscillatory rheological measurements were performed in the linear viscoelastic region. The strain was kept at 0.03%, and a dynamic frequency sweep from 0.1 to 10 rad/s was conducted to measure the storage modulus G' and loss modulus G''. The viscosity was monitored while the stress was increased (frequency = 1 Hz). Measurements were performed in triplicate with 10 min between cycles. The gel recoverability was assessed using no time break between cycles. The statistical analysis was carried out with a one-way ANOVA test first, followed by Dunn's multiple comparisons test. For fluorescence imaging, 10 μL NC-gel was dropped onto the glass slide followed by covering it with a coverslip. The slide was then blocked with nail polish. The sample was imaged on Olympus FV1000 confocal microscope. To study hydrogel morphology, NC-gel was lyophilized and the flake of the gel was placed on a silicon wafer. The sample was coated with iridium and then examined with SEM (FEI XL30 SFEG).

RBC-NP Retention Study. To study retention of RBC-NPs within the NC-gel, the RBC-NPs were labeled with a fluorescent dye DiD. The resulting NC-gel (500 μL) was loaded into a micro-equilibrium dialyzer (Harvard Apparatus), and membrane filters (Whatman, nuclepore track-etch membrane) with the pore size of 1 μm in diameter were used for dialysis against 1 L water. At predetermined time points, 250 μL of water outside of the chamber was taken, and the fluorescence intensity was measured. RBC-NP suspension (10% w/v, 500 μL) without Chi-NPs was used as a control. RBC-NP retention was also studied *in vivo*. Specifically, prior to the study, the back of the mice (six week old male ICR mice from Envigo, n = 3) was carefully shaved. Then 50 μL of DiD-labeled NC-gel was injected subcutaneously to the left flanks of the mice. As a control, RBC-NP suspension (10% w/v, 50 μL) without Chi-NPs was used and injected subcutaneously to the right flanks of the same mice. For live whole-body imaging, mice were anesthetized with isoflurane at designated time points (days 0, 1, 2, and 3) and imaged with a Xenogen IVIS 200 system. For *in vivo* imaging, region of interest (ROI) was generated with Living Image Software immediately after injection. Specifically, ROI was defined as a circular area centered at emission maximum with a radius at 50% cutoff of the emission maximum. The fluorescence intensity in the ROI of the NC-gel group immediately after the injection (day 0) was used as 100%. In all images, fluorescent intensity was quantified with the same ROI centered at emission maximum. Identical settings (lamp voltage, filters, f/stop, fields of view, binning) were used for acquiring all images. Fluorescence intensities were quantified and normalized across the time points. Heat maps were overlaid on bright-field images. All animal experiments followed protocols that were reviewed, approved, and performed under the regulatory supervision of the University of California San Diego's institutional biosafety program and the Institutional Animal Care and Use Committee (IACUC). Statistical analysis was performed with GraphPad Prism using an unpaired two-tailed t test.

Expression and Purification of Recombinant Streptolysin O. The *slo* gene was cloned into vector pET15b and transformed into BL21 DE3 *Escherichia coli*. Bacteria expressing SLO were cultured in 1 L of Luria–Bertani broth and incubated at 37 °C with shaking. Expression was induced in cultures at 0.7 A_{600} with 0.5 mm isopropyl 1-thio-β-D-galactopyranoside (Bio-Vectra) and maintained at 30 °C for 4 h. Bacterial pellets were disrupted by sonication, and soluble 6× histidine-tagged SLO was purified using nickel-nitrilotriacetic acid agarose (Invitrogen). Fractions corresponding to the full-length SLO were pooled, and further purification was achieved using Amicon Ultra centrifugal filters (Millipore Sigma). Protein was monitored by SDS-PAGE and quantitated by A_{280} and frozen in aliquots at −80 °C. Assays were performed in the presence of 10 mm DTT for reducing conditions.

Group A *Streptococcus* Culture. GAS (M1 5448) bacteria were inoculated from a frozen stock to Todd-Hewitt agar plates and cultured for 12 h at 37 °C. Following the culture, a single colony was selected and inoculated to 8 mL of Todd-Hewitt broth (THB). After an overnight culture, 4 mL of the bacterial medium was reconstituted with 250 mL of fresh THB medium, and the culture was continued until the optical density value at 600 nm (OD_{600}) reached 0.4,

DOI: 10.1021/acsnano.7b06968
ACS Nano XXXX, XXX, XXX−XXX

corresponding to 0.8 × 10^8 CFU/mL. The bacteria were then collected with centrifugation (4000*g* for 5 min) and washed twice with PBS.

SLO Neutralization Study. SLO hemolytic activity was first studied. Sixty microliters of SLO (containing 10 mM DTT) with varied concentration was incubated with 0.1 mL of 5% purified human RBCs at 37 °C for 30 min. The concentration of SLO to induce 100% hemolysis was determined when the percentage of the released hemoglobin reached the same level as the lysate from the same amount of RBCs. To evaluate SLO neutralization by the NC-gel *in vitro*, 1.6 μL of SLO solution (0.1 mg/mL containing 10 mM of DTT) was mixed with 59 μL of NC-gel, free RBC-NPs, and PBS. Then 0.1 mL of 5% purified human RBCs was added to each sample, followed by incubation at 37 °C for 30 min. The samples were carefully centrifuged, and the extent of RBC lysis was quantified by measuring the absorption of the supernatants at 540 nm. All experiments were performed in triplicate. Statistical analysis was performed with GraphPad Prism using an unpaired two-tailed *t* test. To study neutralization of SLO by the NC-gel *in vivo*, 100 μL of SLO solution (0.6 mg/mL, containing 10 mM of DTT) was mixed with 100 μL of NC-gel, and the mixture was injected subcutaneously with 19 gauge hypodermic needle into the flank region of 6 week old male ICR mice (Envigo, n = 3). Three other groups, including SLO mixed with free RBC-NPs, SLO toxin alone, and PBS, were used as controls. After 72 h, the lesion was photographed. Then the mice were sacrificed, and the skin and muscle samples were removed. The tissues were frozen, cut, and stained with hematoxylin and eosin (H&E) for histological analysis (Hamamatsu Nanozoomer).

Antivirulence Efficacy against Localized GAS Subcutaneous Infection. Prior to the study, the flanks of 18 ICR mice (6 week old male, Envigo) were carefully shaved. Then a challenge dose of 2 × 10^9 CFU of GAS M1 5448 suspended in 100 μL of PBS was injected subcutaneously into the flank region. Then the mice were randomly divided into three groups (n = 6 per group). For the treatment group, 0.1 mL of NC-gel was injected into the infection region. For the control groups, free RBC-NPs or PBS was injected. The progression of infection in each mouse was carefully monitored and measured for 3 days, with serial photographic image capture and lesion size measurement using ImageJ software. Statistical analysis was performed with two-way ANOVA followed by Tukey posthoc test in GraphPad Prism.

ASSOCIATED CONTENT

Supporting Information

The Supporting Information is available free of charge on the ACS Publications website at DOI: 10.1021/acsnano.7b06968.

Effect of ionic strength on the storage modulus G' and loss modulus G'' of NC-gel; shape stability of NC-gel; statistical analysis of viscosity measurements; statistical analysis of viscosity recovery measurements (PDF)

AUTHOR INFORMATION

Corresponding Author

*E-mail: zhang@ucsd.edu.

ORCID

Karen Christman: 0000-0002-6179-898X

Liangfang Zhang: 0000-0003-0637-0654

Notes

The authors declare no competing financial interest.

ACKNOWLEDGMENTS

This work is supported by the Defense Threat Reduction Agency Joint Science and Technology Office for Chemical and Biological Defense under Grant Numbers HDTRA1-14-1-0064 (to L.Z) and HDTRA1-16-1-0013 (to L.Z.) and NIH Grant R01AI077780 (to V.N.).

REFERENCES

(1) Zaccarelli, E. Colloidal Gels: Equilibrium and Non-Equilibrium Routes. *J. Phys.: Condens. Matter* **2007**, *19*, 323101.

(2) Joshi, Y. M. Dynamics of Colloidal Glasses and Gels. *Annu. Rev. Chem. Biomol. Eng.* **2014**, *5*, 181−202.

(3) Lu, P. J.; Weitz, D. A. Colloidal Particles: Crystals, Glasses, and Gels. *Annu. Rev. Condens. Matter Phys.* **2013**, *4*, 217−233.

(4) Kamata, H.; Li, X.; Chung, U. I.; Sakai, T. Design of Hydrogels for Biomedical Applications. *Adv. Healthcare Mater.* **2015**, *4*, 2360−2374.

(5) Gao, W.; Zhang, Y.; Zhang, Q. Z.; Zhang, L. Nanoparticle-Hydrogel: A Hybrid Biomaterial System for Localized Drug Delivery. *Ann. Biomed. Eng.* **2016**, *44*, 2049−2061.

(6) Appel, E. A.; Tibbitt, M. W.; Webber, M. J.; Mattix, B. A.; Veiseh, O.; Langer, R. Self-Assembled Hydrogels Utilizing Polymer-Nanoparticle Interactions. *Nat. Commun.* **2015**, *6*, 6295.

(7) Diba, M.; Wang, H. N.; Kodger, T. E.; Parsa, S.; Leeuwenburgh, S. C. G. Highly Elastic and Self-Healing Composite Colloidal Gels. *Adv. Mater.* **2017**, *29*, 1604672.

(8) Wang, Q.; Wang, J. X.; Lu, Q. H.; Detamore, M. S.; Berkland, C. Injectable Plga Based Colloidal Gels for Zero-Order Dexamethasone Release in Cranial Defects. *Biomaterials* **2010**, *31*, 4980−4986.

(9) Gu, Z.; Aimetti, A. A.; Wang, Q.; Dang, T. T.; Zhang, Y. L.; Veiseh, O.; Cheng, H.; Langer, R. S.; Anderson, D. G. Injectable Nano-Network for Glucose-Mediated Insulin Delivery. *ACS Nano* **2013**, *7*, 4194−4201.

(10) Wang, Q.; Wang, L. M.; Detamore, M. S.; Berkland, C. Biodegradable Colloidal Gels as Moldable Tissue Engineering Scaffolds. *Adv. Mater.* **2008**, *20*, 236−239.

(11) Wang, Q.; Gu, Z.; Jamal, S.; Detamore, M. S.; Berkland, C. Hybrid Hydroxyapatite Nanoparticle Colloidal Gels Are Injectable Fillers for Bone Tissue Engineering. *Tissue Eng., Part A* **2013**, *19*, 2586−2593.

(12) Kim, B. Y. S.; Rutka, J. T.; Chan, W. C. W. Current Concepts: Nanomedicine. *N. Engl. J. Med.* **2010**, *363*, 2434−2443.

(13) Bobo, D.; Robinson, K. J.; Islam, J.; Thurecht, K. J.; Corrie, S. R. Nanoparticle-Based Medicines: A Review of Fda-Approved Materials and Clinical Trials to Date. *Pharm. Res.* **2016**, *33*, 2373−2387.

(14) Hu, C. M. J.; Zhang, L.; Aryal, S.; Cheung, C.; Fang, R. H.; Zhang, L. Erythrocyte Membrane-Camouflaged Polymeric Nanoparticles as a Biomimetic Delivery Platform. *Proc. Natl. Acad. Sci. U. S. A.* **2011**, *108*, 10980−10985.

(15) Hu, C. M. J.; Fang, R. H.; Copp, J.; Luk, B. T.; Zhang, L. A Biomimetic Nanosponge That Absorbs Pore-Forming Toxins. *Nat. Nanotechnol.* **2013**, *8*, 336−340.

(16) Hu, C. M. J.; Fang, R. H.; Wang, K. C.; Luk, B. T.; Thamphiwatana, S.; Dehaini, D.; Nguyen, P.; Angsantikul, P.; Wen, C. H.; Kroll, A. V.; Carpenter, C.; Ramesh, M.; Qu, V.; Patel, S. H.; Zhu, J.; Shi, W.; Hofman, F. M.; Chen, T. C.; Gao, W.; Zhang, K.; Chien, S.; Zhang, L. Nanoparticle Biointerfacing by Platelet Membrane Cloaking. *Nature* **2015**, *526*, 118−121.

(17) Luk, B. T.; Hu, C. M. J.; Fang, R. N. H.; Dehaini, D.; Carpenter, C.; Gao, W.; Zhang, L. Interfacial Interactions between Natural Rbc Membranes and Synthetic Polymeric Nanoparticles. *Nanoscale* **2014**, *6*, 2730−2737.

(18) Fang, R. H.; Hu, C. M. J.; Luk, B. T.; Gao, W.; Copp, J. A.; Tai, Y. Y.; O'Connor, D. E.; Zhang, L. Cancer Cell Membrane-Coated Nanoparticles for Anticancer Vaccination and Drug Delivery. *Nano Lett.* **2014**, *14*, 2181−2188.

(19) Parodi, A.; Quattrocchi, N.; van de Ven, A. L.; Chiappini, C.; Evangelopoulos, M.; Martinez, J. O.; Brown, B. S.; Khaled, S. Z.; Yazdi, I. K.; Enzo, M. V.; Isenhart, L.; Ferrari, M.; Tasciotti, E. Synthetic Nanoparticles Functionalized with Biomimetic Leukocyte Membranes Possess Cell-Like Functions. *Nat. Nanotechnol.* **2012**, *8*, 61−68.

(20) Gao, W.; Fang, R. H.; Thamphiwatana, S.; Luk, B. T.; Li, J. M.; Angsantikul, P.; Zhang, Q. Z.; Hu, C. M. J.; Zhang, L. Modulating Antibacterial Immunity *Via* Bacterial Membrane-Coated Nanoparticles. *Nano Lett.* **2015**, *15*, 1403−1409.

DOI: 10.1021/acsnano.7b06968
ACS Nano XXXX, XXX, XXX−XXX

(21) Gao, W.; Zhang, L. Engineering Red-Blood-Cell-Membrane-Coated Nanoparticles for Broad Biomedical Applications. *AIChE J.* **2015**, *61*, 738−746.
(22) Hu, C. M. J.; Fang, R. H.; Luk, B. T.; Zhang, L. Nanoparticle-Detained Toxins for Safe and Effective Vaccination. *Nat. Nanotechnol.* **2013**, *8*, 933−938.
(23) Wei, X.; Gao, J.; Wang, F.; Ying, M.; Angsantikul, P.; Kroll, A. V.; Zhou, J.; Gao, W.; Lu, W.; Fang, R. H.; Zhang, L. In Situ Capture of Bacterial Toxins for Antivirulence Vaccination. *Adv. Mater.* **2017**, *29*, 1701644.
(24) Chen, W. S.; Zhang, Q. Z.; Luk, B. T.; Fang, R. H.; Liu, Y. N.; Gao, W.; Zhang, L. Coating Nanofiber Scaffolds with Beta Cell Membrane to Promote Cell Proliferation and Function. *Nanoscale* **2016**, *8*, 10364−10370.
(25) Li, L. L.; Xu, J. H.; Qi, G. B.; Zhao, X. Z.; Yu, F. Q.; Wang, H. Core-Shell Supramolecular Gelatin Nanoparticles for Adaptive and "on-Demand" Antibiotic Delivery. *ACS Nano* **2014**, *8*, 4975−4983.
(26) Wang, F.; Gao, W.; Thamphiwatana, S.; Luk, B. T.; Angsantikul, P.; Zhang, Q. Z.; Hu, C. M. J.; Fang, R. H.; Copp, J. A.; Pornpattananangkul, D.; Lu, W. Y.; Zhang, L. Hydrogel Retaining Toxin-Absorbing Nanosponges for Local Treatment of Methicillin-Resistant Staphylococcus Aureus Infection. *Adv. Mater.* **2015**, *27*, 3437−3443.
(27) Copp, J. A.; Fang, R. H.; Luk, B. T.; Hu, C. M. J.; Gao, W.; Zhang, K.; Zhang, L. Clearance of Pathological Antibodies Using Biomimetic Nanoparticles. *Proc. Natl. Acad. Sci. U. S. A.* **2014**, *111*, 13481−13486.
(28) Wang, Q.; Jamal, S.; Detamore, M. S.; Berkland, C. Plga-Chitosan/Plga-Alginate Nanoparticle Blends as Biodegradable Colloidal Gels for Seeding Human Umbilical Cord Mesenchymal Stem Cells. *J. Biomed. Mater. Res., Part A* **2011**, *96A*, 520−527.
(29) Gao, W.; Vecchio, D.; Li, J. M.; Zhu, J. Y.; Zhang, Q. Z.; Fu, V.; Li, J. Y.; Thamphiwatana, S.; Lu, D. N.; Zhang, L. Hydrogel Containing Nanoparticle-Stabilized Liposomes for Topical Antimicrobial Delivery. *ACS Nano* **2014**, *8*, 2900−2907.
(30) Buffalo, C. Z.; Bahn-Suh, A. J.; Hirakis, S. P.; Biswas, T.; Amaro, R. E.; Nizet, V.; Ghosh, P. Conserved Patterns Hidden within Group a Streptococcus M Protein Hypervariability Recognize Human C4b-Binding Protein. *Nat. Microbiol.* **2016**, *1*, 16155.
(31) Stewart, C. M.; Buffalo, C. Z.; Valderrama, J. A.; Henningham, A.; Cole, J. N.; Nizet, V.; Ghosh, P. Coiled-Coil Destabilizing Residues in the Group a Streptococcus M1 Protein Are Required for Functional Interaction. *Proc. Natl. Acad. Sci. U. S. A.* **2016**, *113*, 9515−9520.
(32) Walker, M. J.; Barnett, T. C.; McArthur, J. D.; Cole, J. N.; Gillen, C. M.; Henningham, A.; Sriprakash, K. S.; Sanderson-Smith, M. L.; Nizet, V. Disease Manifestations and Pathogenic Mechanisms of Group a Streptococcus. *Clin. Microbiol. Rev.* **2014**, *27*, 264−301.
(33) Humar, D.; Datta, V.; Bast, D. J.; Beall, B.; De Azavedo, J. C. S.; Nizet, V. Streptolysin S and Necrotising Infections Produced by Group G Streptococcus. *Lancet* **2002**, *359*, 124−129.
(34) Zhu, H.; Liu, M. Y.; Sumby, P.; Lei, B. F. The Secreted Esterase of Group a Streptococcus Is Important for Invasive Skin Infection and Dissemination in Mice. *Infect. Immun.* **2009**, *77*, 5225−5232.
(35) Zhang, Y.; Zhang, J. H.; Chen, W. S.; Angsantikul, P.; Spiekermann, K. A.; Fang, R. H.; Gao, W.; Zhang, L. Erythrocyte Membrane-Coated Nanogel for Combinatorial Antivirulence and Responsive Antimicrobial Delivery against Staphylococcus Aureus Infection. *J. Controlled Release* **2017**, *263*, 185−191.
(36) Fang, R. N. H.; Hu, C. M. J.; Chen, K. N. H.; Luk, B. T.; Carpenter, C. W.; Gao, W.; Li, S. L.; Zhang, D. E.; Lu, W. Y.; Zhang, L. Lipid-Insertion Enables Targeting Functionalization of Erythrocyte Membrane-Cloaked Nanoparticles. *Nanoscale* **2013**, *5*, 8884−8888.
(37) Kim, J.; Li, W. A.; Choi, Y.; Lewin, S. A.; Verbeke, C. S.; Dranoff, G.; Mooney, D. J. Injectable, Spontaneously Assembling, Inorganic Scaffolds Modulate Immune Cells in Vivo and Increase Vaccine Efficacy. *Nat. Biotechnol.* **2014**, *33*, 64−72.

DOI: 10.1021/acsnano.7b06968
ACS Nano XXXX, XXX, XXX−XXX